RSC Advances

PAPER

View Article Online
View Journal | View Issue

Cite this: *RSC Adv.*, 2026, **16**, 144

Development of novel biochar derived from *Bacopa monnieri* leaves for adsorptive removal of pendimethalin herbicide from binary and ternary pesticide mixture

Shreya Thakor,†[a] Gautam Priyadarshi,†[b] Bhakti Patel,[b] Santosh Kumar Sahu,[b] Sherzodbek Tashbaev,[c] Gulomov Gafurjon Shavkatbek Ugli,[d] Esha Rami, *[a] Dipak Kumar Sahoo *[e] and Ashish Patel *[b]

This study aims to develop and evaluate a sustainable biochar adsorbent derived from *Bacopa monnieri* leaves (BMBC) for the removal of the herbicide pendimethalin (PND) from aqueous solution and pesticide mixtures. The research focuses on studying the adsorption behavior, optimizing parameters, and elucidating the underlying mechanism. BMBC was synthesized through pyrolysis at 600 °C for 2 hours under limited oxygen conditions for the adsorptive removal of pendimethalin (PND) herbicide from an aqueous solution. The materials were characterized using XRD for elemental composition and crystallinity, SEM analysis for size & surface microstructure, and FTIR for identification of functional groups. BMBC exhibits an amorphous carbon structure with minor crystalline peaks (XRD), porous morphology (SEM), and oxygenated functional groups (FTIR). The PND removal experiments were conducted with various parameters, including initial concentration (30–70 mg L^{-1}), contact time (0–150 min), pH (2–12), and absorbent dose (2.5–20 mg). Optimum removal (97.56%) was observed at an equilibrium time of 120 min, at a concentration of 40 mg L^{-1}, pH 8, and a dosage of 5 mg, and ionic interactions were significantly enhanced in the presence of multivalent salts. The combination of profenocombi and PND was removed most effectively (73%) compared to other pesticide mixtures. The adsorption process, governed by pseudo-second-order kinetics (R^2 > 0.98), suggested chemisorption. The Langmuir isotherm model represents high adsorption capacity (q_m) of 82 mg g^{-1}. The adsorption of PND onto BMBC occurs through hydrogen bonding, π–π stacking, electrostatic interaction, and pore filling. This study reveals the potential of BMBC as a highly effective, low-cost, and eco-friendly adsorbent for the removal of PND.

Received 27th September 2025
Accepted 15th December 2025

DOI: 10.1039/d5ra07351k

rsc.li/rsc-advances

1 Introduction

Pesticides are chemical compounds used as insecticides, fungicides, herbicides, and nematicides. While they play a critical role in agricultural development by preventing crop losses, excessive use can lead to harmful effects on the environment and human health. Most pesticides are non-biodegradable, making them a significant source of water contamination.[1] The uncontrolled use of herbicides by farmers is a major concern for scientists and environmentalists worldwide, due to their harmful effects on humans, animals, and microorganisms. The extensive application of that chemical has resulted in water body contamination from a variety of sources, including production facilities, herbicide containers, and damage from leaching and runoff on farms. The toxicity, mutagenicity, and carcinogenicity of herbicides make them extremely hazardous to aquatic life.[2]

Pendimethalin (*N*-1-ethylpropyl-2,6-dinitro-3,4-xylidine) is a dinitroaniline class of herbicide used to regulate perennial grass plants and certain weeds that grow in crops. Pendimethalin (PND) is used as a water-soluble powder, in an emulsifiable quantity, or dispersed granule form.[3] PND is applied in various ways and is frequently used to control weeds in crops, including vegetables, cotton, soybeans, peanuts, maize, rice,

[a]*Department of Life Sciences, Parul Institute of Applied Science, Parul University, Vadodara 391760, Gujarat, India. E-mail: shreyathakor0823@gmail.com; esha.rami82036@paruluniversity.ac.in*

[b]*Department of Life Sciences, Hemchandracharya North Gujarat University, Patan 384265, Gujarat, India. E-mail: priyadarshigautam411@gmail.com; bhaktipatel2233@gmail.com; santoshsahu.hngu@gmail.com; uni.ashish@gmail.com*

[c]*Department of Biology, Andijan State University, Andijan, Uzbekistan. E-mail: sherzodbektashbaev@gmail.com*

[d]*Department of Genetics and Biotechnology, Andijan State University, Andijan, Uzbekistan. E-mail: gulomovgafur47@gmail.com*

[e]*Department of Veterinary Clinical Sciences, College of Veterinary Medicine, Iowa State University, Ames, Iowa, USA. E-mail: dsahoo@iastate.edu*

† These authors contributed equally and share the first authorship.

and wheat. The whole crop's growing phase may be included in the effective period, which can last up to 45–60 days.[4] PND exhibits strong adsorption to soil, high vapor pressure, and limited solubility in water. Consequently, these compounds are prone to surface runoff and volatilization. However, in regions of soil erosion, the previously immobilized insecticide may become mobilized and be transported along with the eroded debris.[5]

Biochar, typically produced through the pyrolysis of biomass, possesses potential catalytic properties due to its multiple functional characteristics, including a large surface area, a porous structure, and a unique chemical composition. The structural and functional attributes are influenced by the conditions of the pyrolysis process.[6] A highly popular technique for creating biochar is pyrolysis, which involves thermochemically reducing biomass. The biomass heated up in an atmosphere with a shortage of oxygen to a temperature between 200 and 1300 °C.[7] The high specific surface areas and large pore sizes inherent to biochar enable physical absorption, hydrophobic interactions, and electrostatic attraction with a wide range of contaminants.[8] Owing to these advantages, biochar-based materials have been investigated for environmental remediation.[9]

Despite numerous studies[10] on biochar-based removal of pesticides, most investigations have focused on single-pollutant systems, generic biomass sources, or modified carbons,[11] while a systematic evaluation of PND removal using unmodified plant-derived biochar remains limited. Previous studies have not reported the combined effect of solution chemistry, ionic strength, and competitive adsorption in multi-pesticide environments, which are more representative of agricultural runoff. Moreover, there is limited information available on the adsorption mechanism of PND, particularly regarding the surface functionality of adsorbents derived from *B. monnieri*, a medicinal plant rich in oxygenated functional groups.

Thus, the present study bridges these gaps by developing a novel *Bacopa monnieri* leaf-derived biochar (BMBC) and systematically evaluating its adsorption performance under both single and mixed pesticide systems. The main objectives were (i) to synthesize biochar from *B. monnieri* leaves *via* pyrolysis at 600 °C for 2 hours; (ii) to characterize the structural and elemental properties of the synthesized biochar using Scanning Electron Microscopy (SEM), Fourier Transformed Infrared Spectroscopy (FTIR), and X-Ray Diffraction (XRD); (iii) to evaluate the removal of PND under various concentrations, pH levels, doses, contact durations; (iv) to investigate the ionic strengths, and competing pesticides in binary and ternary mixtures of pesticides; (v) to model the adsorption process using isotherm and kinetics analysis to understand the removal mechanism better. (vi) Propose a mechanism pathway describing the interaction responsible for PND removal.

2 Materials and methods

2.1 Materials

Bacopa monnieri (*B. monnieri*), commonly known as Brahmi (leaf) powder collected from the local market of Patan, Gujarat. Magnesium carbonate ($MgCO_3$), sodium chloride (NaCl), calcium carbonate ($CaCO_3$), zinc phosphate ($ZnSO_4$), hydrochloric acid (HCl), Sodium hydroxide (NaOH), and potassium chloride (KCl) were high-purity reagent products from Sisco Research Laboratories (SRL) Pvt. Ltd, Mumbai, India. Pendimethalin herbicide collected from TATA Panida, India. Profenocombi (profenofos + cypermethrin) collected from Molraxa Agro Chemicals, Ahmedabad, Gujarat, and H-twenty (chlorpyrifos) collected from Hakuba Organics Pvt. Ltd, Ahmedabad, Gujarat. A list of detailed chemicals, instrument parameters, and biochar preparation conditions is given in Tables S4–S6.

2.2 Synthesis of biochar

The dried leaves of *B. monnieri* were ground and sieved through a 100-mesh stainless steel sieve (<150 μm) to obtain a uniformed particle size. Approximately 10 g of this powder was placed in a covered quartz crucible to limit the air exposure and then transferred to a muffle furnace for pyrolysis. The pyrolysis was carried out at 600 °C for 2 hours under limited oxygen concentration. The furnace was heated at a rate of 10 °C min^{-1} until the target temperature was reached. The internal pressure was maintained at near-ambient levels (1 atm). After the residence time, the crucible was allowed to cool naturally to room temperature. The resulting carbonized material was gently crushed in an agate mortar, sieved again to remove coarse particles, and stored in an airtight container. The eqn (1) used for calculating biochar yield, which was 21.87% after the pyrolysis.

$$\text{Biochar yeild}(\%) = \frac{\text{weight of biochar}}{\text{weight of biomass}} \times 100 \quad (1)$$

2.3 Characterization of biochar

The XRD spectra of these samples were recorded between specific 2θ values on a D8 Advance (Bruker, Netherlands) instrument to comprehend the crystal structure of the materials. The morphological characterization of BMBC was performed using SEM (FEI Nova NanoSEM 450). FT-IR spectra (S6500 Spectrum Instrument, PerkinElmer, USA) were recorded in the range of 550 to 4000 cm^{-1} to identify the functional groups on the BMBC surface. The point zero charge (pH_{ZPC}) of the BMBC adsorbent was measured using the pH drift method, as described in our previous study,[12] by measuring the initial and final pH values with a pH meter (ELICO LI 617).

2.4 PND removal experiments

Solutions of PND concentrations including 30, 40, 50, 60, and 70 mg L^{-1} were prepared, and 50 mL of each solution was taken in a separate conical flask. 50 mg of BMBC was added to each flask, and agitated for 30, 60, 90, 120, and 150 min at 25 ± 2 °C using a temperature-controlled orbital shaker incubator (REMI CIS-24 BL). After each 30-minute interval, samples were centrifuged at 5000 rpm for 10 min to determine the residual PND concentration using a UV-Vis Spectrophotometer (Labman UV-Vis Double Beam Spectrophotometer – LMSPUV1900). Eqn (2)

and (3) were used for calculating PND removal efficiency (%) and adsorption capacity (q_e) of BMBC (mg g^{-1}).

$$\text{PND removal}(\%) = \frac{(C_0 - C_e)}{C_0} \times 100\% \quad (2)$$

$$\text{PND adsorption capacity}(q_e) = \frac{(C_0 - C_e) \times (V)}{W} \quad (3)$$

where, C_0 = initial concentration, C_e = final concentration, V = volume of PND solution, W = dry weight of BMBC in g.

The effect of pH on PND removal was examined in 10 mL of 40 mg L^{-1} at six distinct pH levels: 2, 4, 6, 8, 10, and 12. The pH of the solutions was maintained using 0.01 M NaOH and 0.1 M HCl solutions. Each PND solution included 10 mg of BMBC and was mixed at room temperature for 150 min. At equilibrium, the final concentration of PND is measured. Under the same conditions at pH 6, the effect of varying BMBC dosages (2.5, 5, 10, and 20 mg) was evaluated in 10 mL of 40 mg per L PND solution.

The adsorption kinetics were investigated using the pseudo-first-order (PFO), pseudo-second order (PSO), and intra-particle diffusion models (IPD). The linear and non-linear equations used for kinetics models are provided in Table S1 of the SI. Three isotherm models (Langmuir, Freundlich, and Temkin) were used to evaluate the fitting of the equilibrium data. The equations for the isothermal models, both linear and non-linear, as listed in Table S2 of the SI. The summary table of adsorption experimental design for PND removal using BMBC is listed in Table S3.

2.5 Ionic strength of BMBC

Using 1 M salt concentrations of $CaCO_3$, NaCl, $ZnSO_4$, $MgCO_3$, and KCl, the ionic strength of BMBC was examined. 1 mL of salt solution (1 M), 1 mL of PND stock solution (400 mg L^{-1}), and 8 mL of deionized water were used to combine each solution (10 mL). 10 mg of BMBC was added to each salt-containing PND solution, and the mixture was shaken for 150 minutes at room temperature. The BMBC was separated from the mixture using centrifugation to calculate the quantity of PND removal in an ionic solution.

2.6 Performance evaluation of PND removal from mixtures of pesticides

The evaluation of the competitive removal study of the PND adsorption of the binary and ternary mixture of different pesticides. The ternary mixture was prepared using PND, profenocombi (PFC) [cypermethrin + profenofos], and H-TWENTY (H-20) [chlorpyriphos]. The mixture of pesticides was prepared in a total of 10 mL by combining 3.3 mL each of the pesticide stock solutions at concentrations of 120 mg L^{-1} and 60 mg L^{-1}, resulting in working solutions with final concentrations of 20 mg L^{-1} and 40 mg L^{-1}, respectively. Likewise, a binary mixture containing (mixture of PND with PFC and PND with H-20) 20 mg L^{-1} and 40 mg L^{-1} was prepared by mixing 5 mL of each stock solution with concentrations 80 mg L^{-1} and 40 mg L^{-1}. 10 mg of BMBC was added to the pesticide mixture containing the tubes, then placed in an incubator shaker and incubated for 150 minutes. After incubation, the tubes were centrifuged at 5000 rpm for 10 min to extract the BMBC. The supernatant was used to determine the residual concentration of PND using a UV-Vis spectrophotometer at wavelengths of 452, 448, and 536 nm. The zero-crossing method was employed to analyze the PND concentration in a mixture of solutions using first- and second-derivative spectra of a mixture of pesticides with PND, as shown in Fig. S1 and S2. Fig. S3 illustrates the derivative spectrophotometric analysis of different PND concentrations and their correlations.[13]

3 Results and discussion

3.1 Characterization of the biochar

3.1.1 XRD analysis of biochar. The crystalline structure of the BMBC was investigated using XRD. Fig. 1 shows the diffraction peak observed at 2θ values ranging from 3 to 90° in continuous scanning mode. Examining the amorphous structure of BMBC and the crystallinity of biomass.[14] However, several examples of distinct, sharp peaks may be observed at a different crystalline structure shown by the two values at 28.36 and 31.7, which are assigned to silicon dioxide (SiO_2; Quartz) corresponding to the (200) plane of pytolith-rich biomass, 40.8 and 45.5, which attribute to potassium (K) containing crystalline phases, correspond to the (220) plane; and the peak at 66.42, which corresponds to the calcite ($CaCO_3$) referred to as the (420) crystallographic plane, commonly retained after pyrolysis. The results of XRD indicate that BMBC has a coexistence of amorphous carbon region with mineral-associated crystalline traces of SiO_2, K, and $CaCO_3$ derived from the parent biomass. Similar crystalline features have been reported in biochar derived from mineral-rich plant residues.[15]

3.1.2 FTIR analysis of biochar. The FTIR spectra of BMBC depicted in Fig. 2, compared before and after PND adsorption (PND-BMBC). The absorption peak at 1031 cm^{-1} represents C–O stretching (standard range: 1000–1100 cm^{-1}), whereas a minor

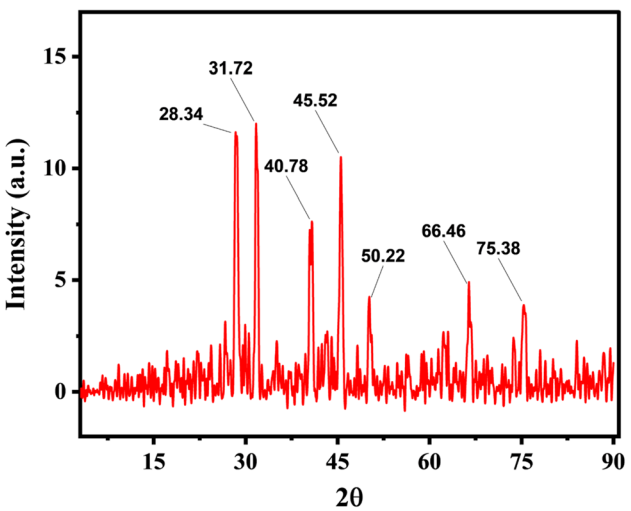

Fig. 1 XRD spectra of BMBC.

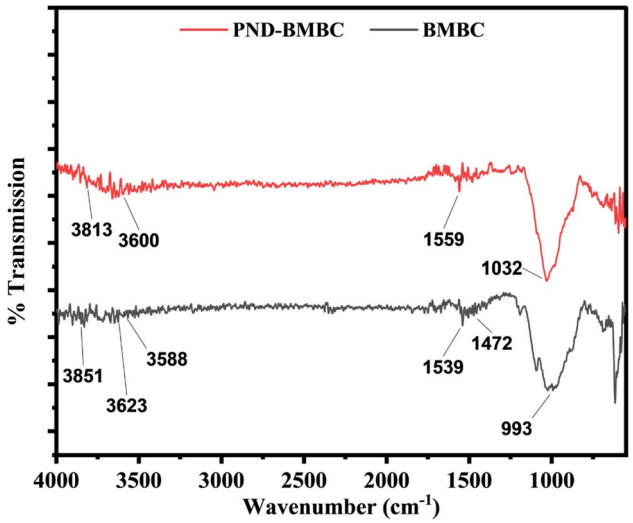

Fig. 2 FTIR of BMBC before (gray colored) and after PND removal, PND-BMBC (red colored).

transition shortly before the 992 cm^{-1} peak, owing to aromatic C–H bending (standard range: 900–1000 cm^{-1}), indicates interaction sites associated with PND adsorption. After loading, the wide and strong peaks at 3588 cm^{-1} (O–H stretching: standard range: 3200–3600 cm^{-1}) and 3623 cm^{-1} (free –OH groups) become less intense, indicating hydrogen bonding. A slow rise before 3600 cm^{-1} and a prominent peak at 3813 cm^{-1} correlate to hydroxyl stretching, which shifted in BMBC-PND. The ridge before 1539 cm^{-1} implies asymmetric $-NO_2$ bending (standard: 1500–1600 cm^{-1}) or aromatic C=C vibrations (standard 1450–1600 cm^{-1}), whereas the peak at 1559 cm^{-1} corresponds to N–H bending or aromatic C=C stretching (standard 1500–1600 cm^{-1}), indicating a strong relationship between PND and BMBC surface functional groups.[16] Furthermore, the peak at 1472 cm^{-1} in BMNC confirmed the presence of amorphous calcium carbonate.

3.1.3 SEM analysis of biochar. Fig. 3a and b represents an SEM image of the synthesized BMBC surface morphological features. Both pictures were captured at a magnification of 25 000× with a scale bar of 3 μm, a voltage of 20.00 kV, and a working distance of 7.0 mm to ensure consistency among observations. The imaging technique reveals that the surface of BMBC is rough, irregular, and highly porous, with uniformly spaced and hard areas containing small nano- to sub-micron particles (approximately 100–500 nm) interspersed with thicker, flake-like structures.[16]

3.2 PND removal experiment

3.2.1 Initial PND concentration and contact time. The removal efficiency (%R) and adsorption capacity (q_e, mg g^{-1}) of PND at various initial concentrations (30–70 mg L^{-1}) and contact time (0 to 150 min) are depicted in Fig. 4a and b. All concentrations exhibit a sharp increase in R% during the first 30 minutes, with 40 mg L^{-1} achieving the maximum removal (76.92%), followed by 30 mg L^{-1} (67.92%) and 50 mg L^{-1} (62.35%). After 90 min, 40 mg L^{-1} rises to 93.03%, whereas 70 mg L^{-1} increases to 64.22%. At 120 min, most concentrations reached equilibrium: 40 mg L^{-1} peaks at 95.29%, while 50 and 60 mg L^{-1} exhibit around 74.80% and 75.51%, respectively. At 150 minutes, 40 mg L^{-1} achieves the maximum removal rate of 97.56%, whereas 30 mg L^{-1} reduces to 65.86%, due to site saturation or desorption. At low concentrations, high forces move PND molecules toward the adsorbent; however, at higher concentrations, lower attraction optimizes their contact with the active sites.[17] In Fig. 4b, q_e increases significantly within the first 30 min, particularly for 70 mg L^{-1} (33.49 mg g^{-1}), 50 mg L^{-1} (31.17 mg g^{-1}), and 40 mg L^{-1} (30.77 mg g^{-1}), while 30 mg L^{-1} remains low (~2.04 mg g^{-1}). Between 60 to 90 min, q_e continues to increase, with 70 mg L^{-1} reaching (44.95 mg g^{-1}), followed by 60 mg L^{-1} (38.31 mg g^{-1}). At 120 minutes, the highest q_e was for 70 mg L^{-1} (45.78 mg g^{-1}), followed by 60 mg L^{-1} (45.30 mg g^{-1}) and 50 mg L^{-1} (37.40 mg g^{-1}). At 150 minutes, q_e for 40 mg L^{-1} increased to 39.02 mg g^{-1}, whereas 70 mg L^{-1} decreased slightly to 42.24 mg g^{-1}. At this time, a slight reduction in q_e might be due to desorption or redistribution. Overall, 40 mg L^{-1} yields the constant and best removal

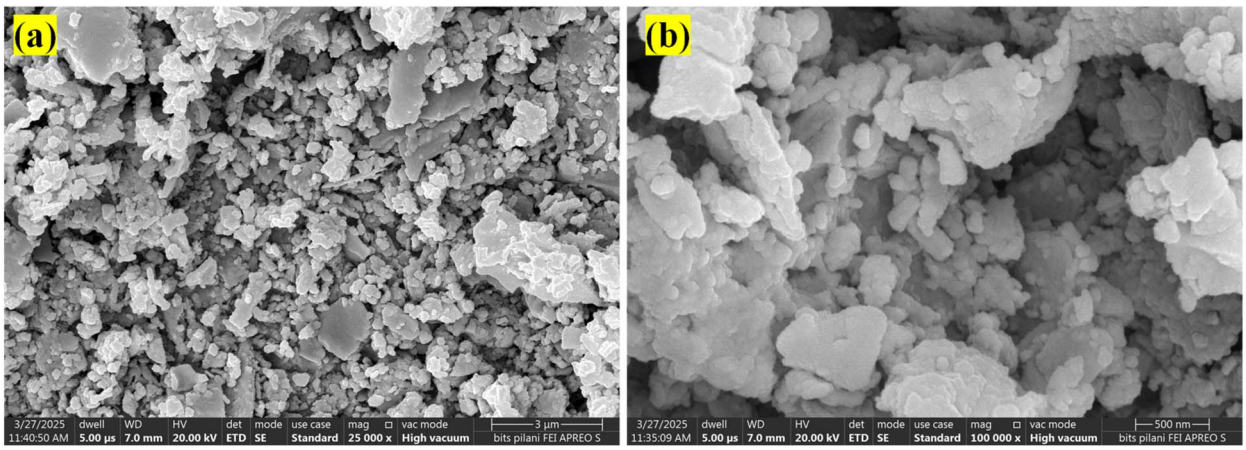

Fig. 3 SEM images of BMBC at magnification of 25 000× (a) and 100 000× (b).

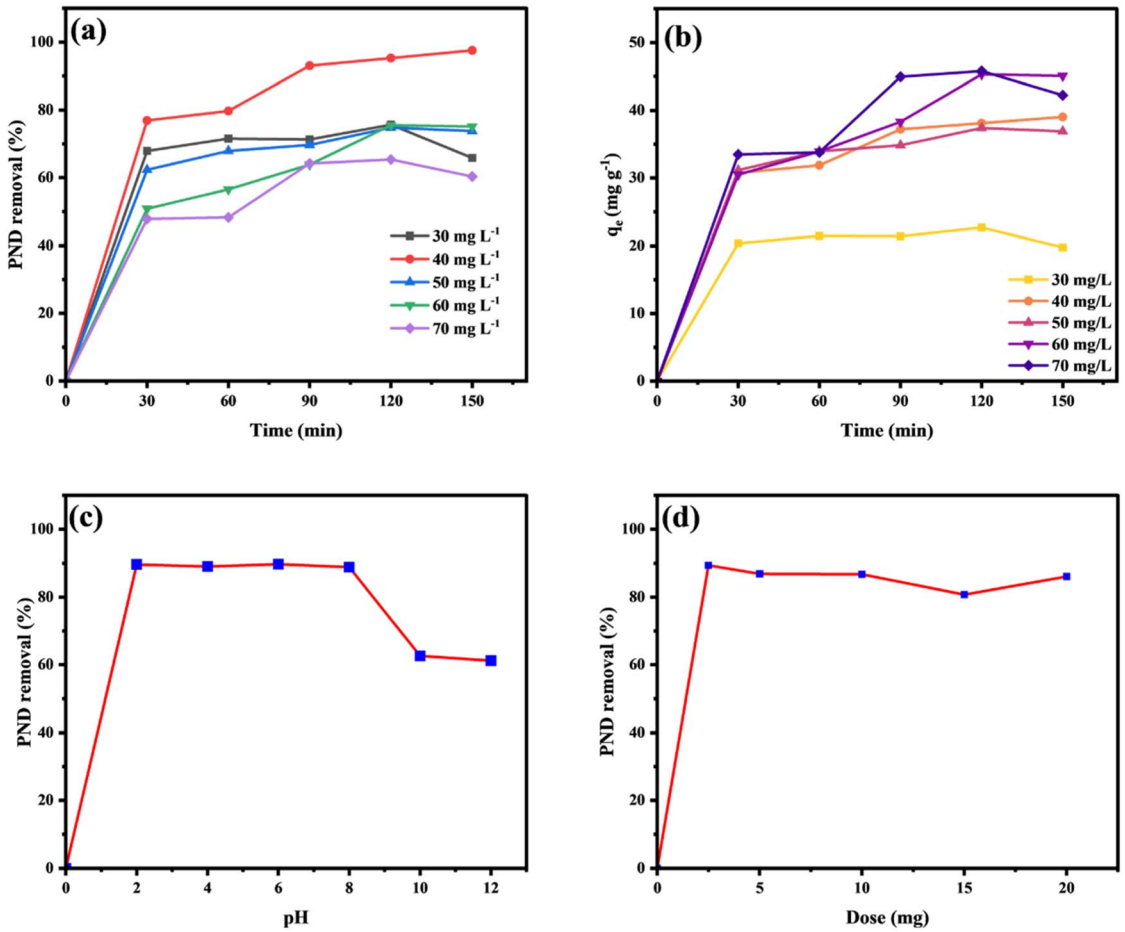

Fig. 4 Adsorption parameters: initial concentration and contact time effect on PND removal % (a), adsorption capacity (b), effect of pH (c), effect of dose (d).

efficiency, while q_e increases proportionately with concentration, due to increased solute availability and diffusion.[18] Concentration curves in Fig. 4a and b appear closely aligned at certain intervals, particularly for the higher initial concentration (50–70 mg L^{-1}). This convergence occurs because the rapid initial adsorption phase is governed by similar mass-transfer and diffusion rates across all concentrations. As the BMBC active sites become progressively saturated, the adsorption rates approach a common limiting value, resulting in the overlapping of removal lines.

3.2.2 Effect of solution pH and pH_{ZPC}. The effect of solution pH on PND removal was examined over a broad pH range (2 to 12), as shown in Fig. 4c. The removal efficiency remained consistently high throughout the entire pH range, reflecting the

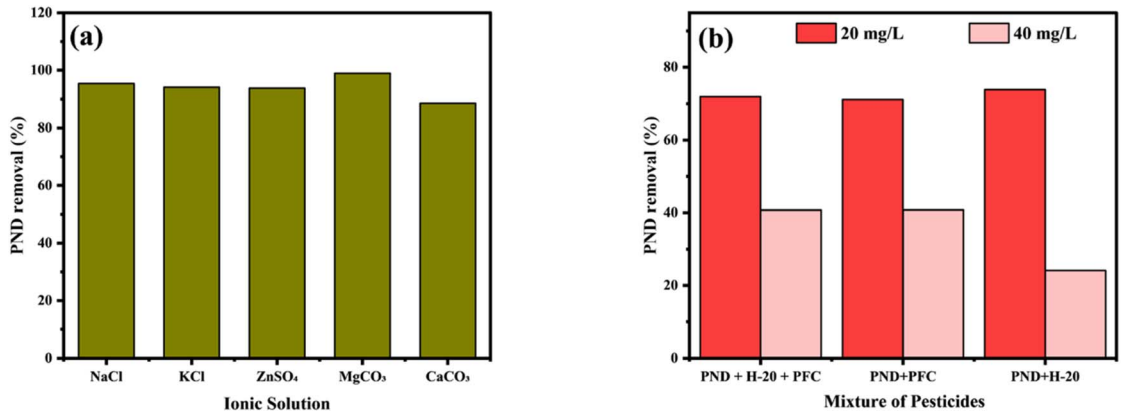

Fig. 5 Effect of ionic solution (a) and PND removal from mixtures of pesticide (b).

robust and pH-tolerant nature of BMBC's adsorption. The adsorbent exhibits exceptional removal efficiency after 150 min, with R% values of ~89% at pH levels ranging from 2 to 8. However, there is a noticeable decrease in removal as the pH level increases into alkaline conditions (pH 10 and 12), decreasing to ~62%. The reduction is attributed to changes in surface charge (highly negative charge at higher pH as pHZPC was 2.07) and increased competition from –OH ions, which reduces the electrostatic interactions towards PND molecules. Additionally, the deprotonation of surface functional group also weakens hydrogen bonding interactions. These combined effects reduce the adsorption capacity at higher pH.[19] At lower pH, reduced competition between PND and hydrogen ions, along with increased positive surface charge, enhanced adsorption. In contrast, at higher pH levels, the surface becomes less positively charged, resulting in reduced PND

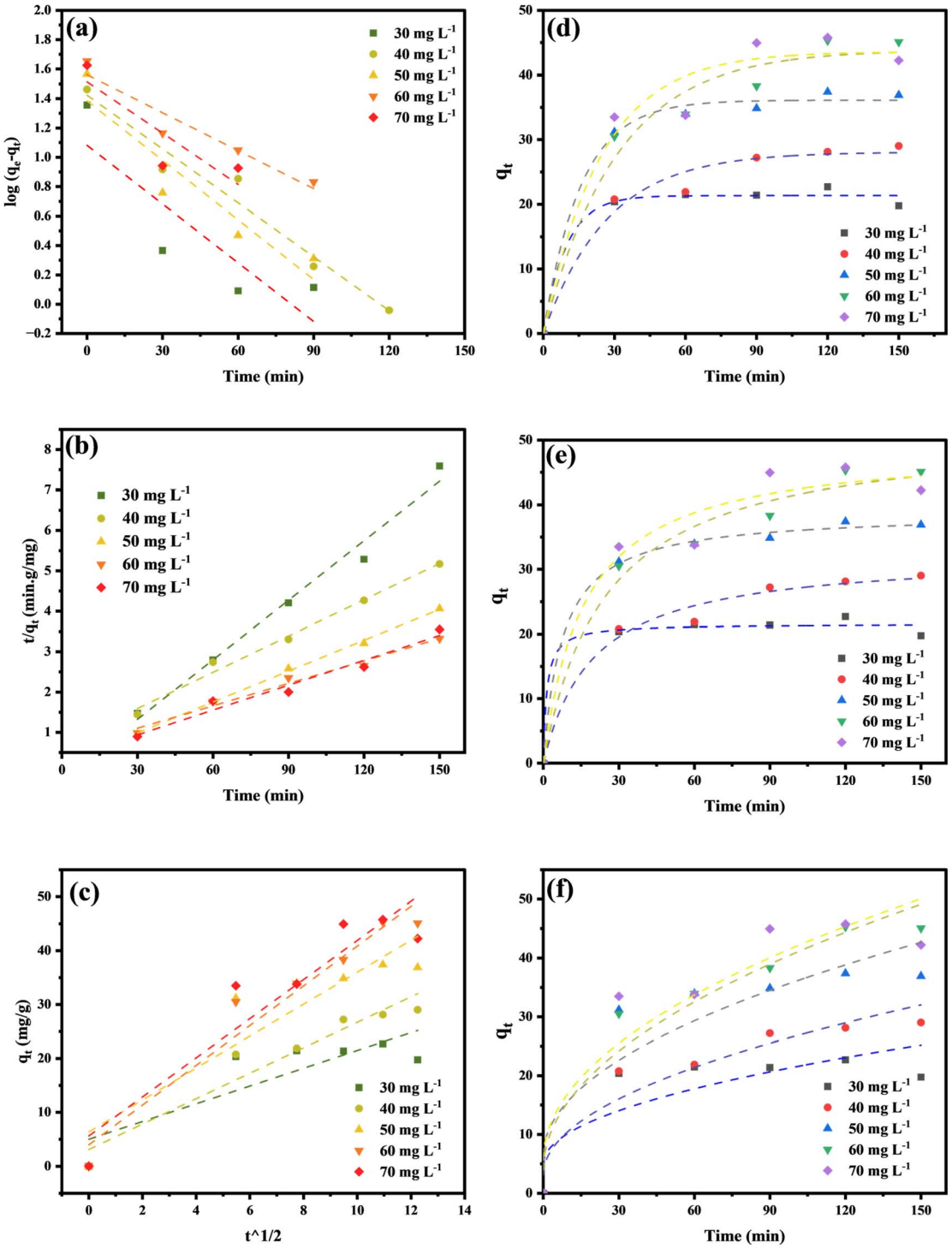

Fig. 6 Linear and non-linear PFO (a and d), PSO (b and e), IPD (c and f) for the removal of PND herbicide onto adsorbent BMBC.

uptake.[20] The result of the pH_{ZPC} of BMBC, illustrated in Fig. S4, shows a point zero charge at a pH of 2.07. At pH levels above pH_{ZPC}, the surface charge of BMBC remained negative across the entire pH range (2–12). The negative charge corresponds to the surface function group, such as –OH, as confirmed in FTIR spectra.

3.2.3 Effect of BMBC dosages. The effects of adsorbent dosage on removal efficiency at 150 minutes are shown in Fig. 4d. The removal efficiency increased significantly to 89.39% with the addition of only 2.5 mg of adsorbent, suggesting high adsorption capacity at low doses. Further increases to 5 mg and 10 mg maintained high efficiency at 86.86% and 86.75%, respectively, suggesting effective utilization of adsorption sites within this range. At 15 mg, the removal efficiency decreased to 80.73%, due to particle aggregation, which reduced the effective surface area available for adsorption. A slight recovery to 86.08% observed at 20 mg, suggesting a minor increase in site availability or diffusion. Overall, these results indicate that the removal efficiency did not consistently increase with increasing adsorbent dosages, suggesting a potential limitation due to adsorbent saturation and particle interaction.[21]

3.2.4 Ionic strength. Fig. 5a represents the effect of various salts ($CaCO_3$, $MgCO_3$, KCl, NaCl, and $ZnSO_4$) on the PND removal efficiency of BMBC, illustrating the role of ions in the adsorption process. The highest percentage of removal, 98.96% was obtained in the presence of $MgCO_3$, indicating a significant increase in adsorption that may be the result of favorable ionic interactions or better adsorbent distribution. High efficiencies of 95.74% and 94.22% are also demonstrated by NaCl and KCl, respectively, suggesting that common monovalent salts significantly improve or preserve adsorption efficiency. A slightly reduced clearance of 93.86% obtained with $ZnSO_4$, possibly because of interaction between the adsorbent surface and Zn ions. On the other hand, $CaCO_3$ had the lowest efficiency at 88.57%. This may be due to surface limiting effects from the ions of calcium or carbonate precipitation. These findings align with the expected cation exchange behavior of PND, with $MgCO_3$ providing the most favorable effect.[22]

3.2.5 Effect of pesticide mixtures. Mixture of pesticides at 40 mg L^{-1} and 20 mg L^{-1} concentrations, the adsorption effectiveness of BMBC was evaluated using the same methods. The result of the effect of the pesticide mixture is depicted in Fig. 5b, where PND + H_2O (73.91%) > PND + H_2O + PFC (71.97%) > PND + PFC (71.16%) was the trend at 20 mg L^{-1}, indicating superior elimination with mixed-structure pesticides. Following PND + H_2O + PFC (40.72%) > PND + PFC (40.77%) > PND + PFC (24.09%), the removal dropped to 40 mg L^{-1}. The decreased efficiency at increasing concentrations suggests potential site saturation. These findings support earlier research showing that the selective adsorption of BMBC is influenced by both pesticide concentration and structure.[23]

3.3 Adsorption kinetics modelling

The rate of PND adsorption onto BMBC at various concentrations (30 to 70 mg L^{-1}) was evaluated using PFO, PSO, and IPD models in linear and non-linear graphs represented in Fig. 6.

Table 1 Linear and non-linear regression of PFO, PSO, and IPD kinetics rate models for the adsorption of PND onto BMBC

	Kinetics models		Linear			Non-linear		
	C_0 (mg g^{-1})	$q_{e(exp)}$ (mg g^{-1})	$q_{(cal)}$ (mg g^{-1})	k_1 (min^{-1})	R^2	$q_{(cal)}$ (mg g^{-1})	k_1 (min^{-1})	R^2
PFO	30	19.759	12.0726	0.0306	0.7509	21.336	0.1039	0.9884
	40	29.024	22.1462	0.0237	0.9264	28.083	0.0370	0.9749
	50	36.903	17.8320	0.0226	0.8658	36.123	0.0632	0.9945
	60	45.090	95.6533	0.7883	0.9308	43.865	0.0321	0.9705
	70	42.238	26.9712	0.0260	0.8567	43.605	0.0480	0.9610

	Kinetics models		Linear			Non-linear		
	C_0 (mg g^{-1})	$q_{e(exp)}$ (mg g^{-1})	$q_{(cal)}$ (mg g^{-1})	k_2 (g mg^{-1} min^{-1})	R^2	$q_{(cal)}$ (mg g^{-1})	k_2 (g mg^{-1} min^{-1})	R^2
PSO	30	19.759	20.6612	0.0331	0.9897	21.572	0.0341	0.9875
	40	29.024	30.1205	0.0334	0.9445	32.3775	0.0015	0.9859
	50	36.903	37.3134	0.0074	0.9988	38.767	0.0033	0.9981
	60	45.090	47.1698	0.0017	0.9998	51.767	7.8031	0.9835
	70	42.238	45.2489	0.0319	0.9901	49.218	0.0012	0.9675

	Kinetics models		Linear			Non-linear		
	C_0 (mg g^{-1})	$q_{e(exp)}$ (mg g^{-1})	K_{diff}	C	R^2	K_{diff}	C	R^2
IPD	30	19.759	0.3752	18.326	0.8668	1.6489	4.9978	0.7109
	40	29.024	1.3611	12.903	0.9144	2.3616	3.0965	0.9246
	50	36.903	0.9054	26.543	0.9299	2.9635	6.3699	0.8354
	60	45.090	2.4069	16.527	0.9433	3.6884	3.9661	0.9468
	70	42.238	2.5937	17.678	0.8146	3.6288	5.6090	0.8777

The kinetic rate parameters at various initial concentrations are shown in Table 1.

The linear PFO model demonstrates moderate to poor fits, with R^2 values (0.7509 to 0.9308). The adsorption capacity $q_{e(cal)}$ was lower or higher than the experimental $q_{e(exp)}$ values. The non-linear PFO fits better with R^2 values (0.9610 to 0.9945) and closer agreement between experimental $q_{e(exp)}$ and model $q_{e(cal)}$ values, as shown in Table 1. Both linear and non-linear PSO models exhibit the best fitting with R^2 values (>0.94) and closed match $q_{e(exp)}$ and $q_{e(cal)}$ values for each concentration. The results revealed the fitting of both models, PFO and PSO, indicating that chemosorption of PND onto BMBC molecules is physically driven.[24,25]

The IPD model shows multi-stage adsorption behavior. The R^2 values (0.7109 to 0.9468) indicate that the intra-particle diffusion was not the only rate-limiting factor. The higher C

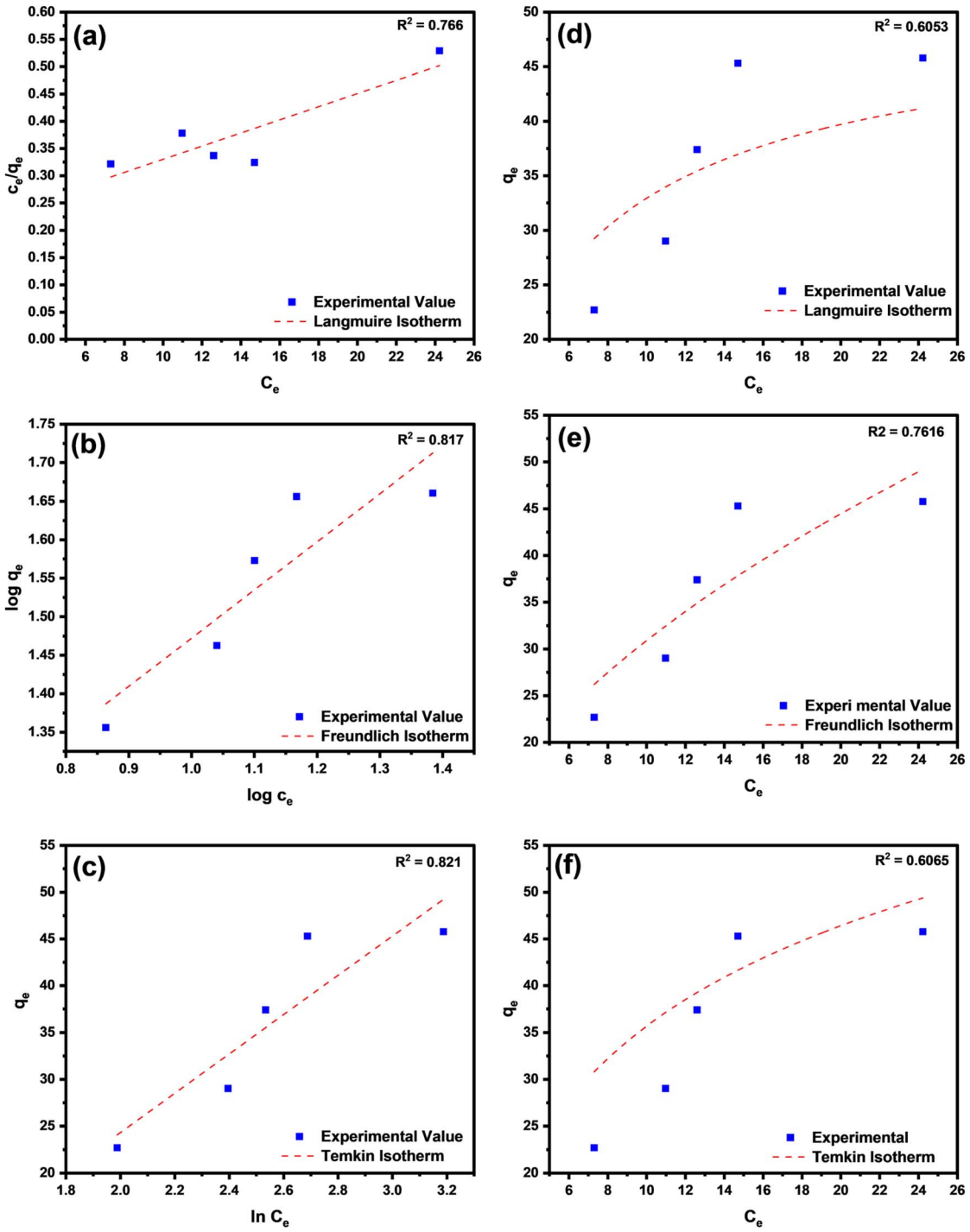

Fig. 7 Linear and non-linear regression of Langmuir isotherm (a and d), Freundlich isotherm (b and e) Temkin isotherm (c and f) for the removal of PND onto BMBC.

Table 2 Linear and non-linear isotherm model parameters

Isotherm model	Isotherm parameters	Linear	Non-linear
Langmuir	q_m (mg g^{-1})	82.64	50.401
	K_L (L g^{-1})	0.0025	0.193
	R^2	0.7663	0.6053
Freundlich	K_F (mg$^{1-1/n}$ L$^{1/n}$ g^{-1})	7.0291	9.2295
	n	1.5993	1.9051
	$1/n$	0.6253	0.5249
	R^2	0.8177	0.7616
Temkin	K_T (L mg^{-1})	0.4314	1.4039
	B_T (J mol^{-1})	20.981	15.496
	R^2	0.8213	0.6065

values confirmed that the boundary layer effect also contributed to the adsorption process. The higher K_{diff} values at 70 mg L^{-1} suggest increased diffusion rates with higher concentrations in the linear fit; yet, persistent C values indicate that external film diffusion also plays a role.[18] The best-fit PSO model in non-linear form, combined with a significant C intercept from the IPD model, indicates that PND adsorption onto BMBC is primarily governed by a chemisorption process involving a boundary layer and intraparticle diffusion.

3.4. Adsorption isotherm modelling

The Langmuir, Freundlich, and Temkin models are used to understand the adsorption behavior at equilibrium. Fig. 7(a–c) shows linear fitting, while Fig. 7(d–f) shows their non-linear regression. Table 2 summarizes the corresponding isotherm parameters, including the linear and non-linear correlation coefficients (R^2) and other parameters, which were determined using the non-linear models in OriginPro software.[26] The Langmuir model represents the achievement of a homogeneous adsorbed monolayer, while the Freundlich model demonstrates the surface's heterogeneity with multilayer adsorption.[27] The Temkin model, on the other hand, describes adsorbate–adsorbent interactions with decreasing adsorption energy.[16] The Langmuir isotherm model exhibits correlation with R^2 values of 0.7663 and 0.6253 for the linear and non-linear models, respectively. The adsorption capacity (q_m) values were 82.64 and 50.40 mg g^{-1}, with a Langmuir constant (K_L) of 0.0025 and 0.193 L g^{-1}, for linear and non-linear, respectively, indicating the absorbate's affinity for the surface. The Freundlich isotherm model yields a reasonable fit in both linear (R^2 = 0.8177) and non-linear (R^2 = 0.7616) forms. The favorable adsorption conditions are further verified by the $1/n$ values in both linear and non-linear forms (0.6253 and 0.5249). The Temkin isotherm for the linear form demonstrated a greater correlation, with K_T = 0.4314 L mg^{-1}, B_T = 20.981 J mol^{-1}, and a higher R^2 = 0.8213, suggesting a significant adsorbent–adsorbate interaction. The Temkin heat of adsorption (B_T) value indicates a moderate binding energy, confirming physisorption. In comparison with the non-linear form provided, the values (K_T = 1.4039 L mg^{-1}, B_T = 15.496 J mol^{-1}, R^2 = 0.6065) indicate a moderate fit. Overall, the Freundlich and Temkin models in their linear forms provide a better fit than the Langmuir model, highlighting the heterogeneity of the BMBC surface and the multilayer adsorption process.[21]

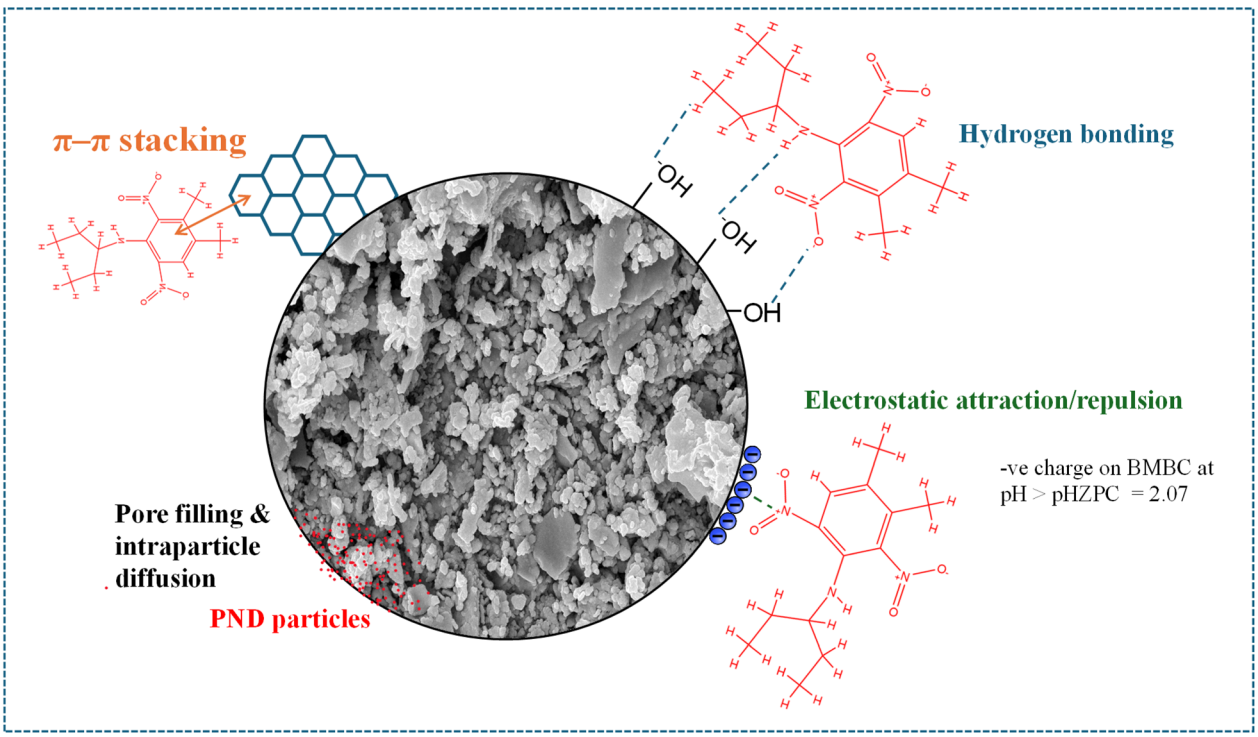

Fig. 8 Proposed mechanism of PND adsorption onto BMBC.

3.5. Mechanism of PND onto BMBC

The adsorption of PND onto BMBC proceeds through a multi-mechanistic pathway, combining π–π stacking, hydrogen bonding, electrostatic interactions, and pore filling, as represented in the proposed mechanism (Fig. 8). Hydrogen bonding between the oxygen-containing functional groups of BMBC (–OH and C–O) and the polar moieties on PND enhances molecular binding. It stabilizes the adsorbent–adsorbate complex, driving the system towards equilibrium. Electrostatic interaction further contributes, arising from the charge or polarity difference between BMBC and PND; this is particularly affected by ionic strength, which can amplify the electrostatic forces.[28] Furthermore, π–π stacking interactions occur through the connection of aromatic structures in BMBC and the aromatic rings of PND molecules. Pore filling complements these mechanisms, as PND molecules diffuse into micro- and mesopores on the BMBC surface and become physically trapped, thereby increasing the effective adsorption capacity.[29] The pore filling contribution to PND adsorption was further supported by isotherm results. The good fitting of the Freundlich isotherm suggests heterogeneous multilayer adsorption, which is associated with micropores and mesopores, confirming the pore-filling behavior. The adsorption of PND onto BMBC proceeds *via* a synergistic mechanism, including: (1) rapid initial uptake through electrostatic interaction and π–π interaction at external active sites, (2) hydrogen bonding, and (3) intraparticle diffusion and pore filling, contributing to the final equilibrium capacity.[30] The combination of heterogeneous surface adsorption, moderate adsorption energies, and chemosorption-influenced kinetics confirmed the PND removal by BMBC governed by multiple co-existing mechanisms.

4 Conclusions

In this study, a novel biochar (BMBC) was synthesized from *Bacopa monnieri* leaf powder *via* pyrolysis at 600 °C for 2 h under limited oxygen conditions. The material characterization confirmed an amorphous carbon structure with minor crystalline phases (XRD), the presence of –OH, C–O, and aromatic groups (FTIR), and a porous surface morphology (SEM), all of which are favorable for adsorption. Batch adsorption experiments revealed that BMBC achieved a maximum PND removal efficiency of 97.56% at pH 8, with an initial PND concentration of 40 mg L^{-1}, an adsorbent dose of 50 mg, and a contact time of 150 min. The adsorption capacity reached 82.64 mg g^{-1} (Langmuir model), and the process followed pseudo-second-order kinetics (R^2 > 0.98), confirming the dominance of chemosorption. The presence of salt influences the removal efficiency, with $MgCO_3$ exhibiting the highest enhancement (98.96%), followed by NaCl (95.71%) and KCl (94.22%). In binary and ternary pesticide mixtures, BMBC removed ~73% PND, demonstrating strong selectivity and surface affinity even under competitive conditions. The proposed adsorption mechanism involved π–π stacking, hydrogen bonding, electrostatic interactions, and pore filling, which together governed the high adsorption efficiency. Overall, BMBC represents an effective, low-cost, and sustainable biochar adsorbent for the removal of pendimethalin and other organic contaminants from aqueous solutions.

Author contributions

S. T. and G. P. writing original draft, formal analysis and investigation, B. P. and S. K. S. writing – review and editing, S. T. and G. G. S. U. validation, writing – review and editing, E. R., D. K. S., and A. P. conceptualization, project administration, resources. All authors read and approved the final manuscript.

Conflicts of interest

The authors declare no competing interests.

Data availability

Data will be made available on request to the corresponding authors.

Supplementary information (SI): technical data, experimental parameters, and spectral analysis for the study on developing *Bacopa monnieri* leaf-derived biochar (BMBC) for the removal of pendimethalin (PND) herbicide. See DOI: https://doi.org/10.1039/d5ra07351k.

Acknowledgements

The authors would like to thank the Department of Life Sciences at Parul University, Vadodara, and the Department of Life Sciences at HNGU, Patan, for the support in conducting this study.

References

1 M. Tudi, H. D. Ruan, L. Wang, J. Lyu, R. Sadler, D. Connell, C. Chu and D. T. Phung, *Int. J. Environ. Res. Public Health*, 2021, **18**, 1112.
2 A. A. Alalwait, M. Khan, I. Khan, I. Ahmad, S. Ballal, G. C. Sharma, R. S. K. Sharma, L. Bareja and M. A. Bajaber, *J. Aust. Ceram. Soc.*, 2025, **61**, 1889–1899.
3 L. Hou, J. L. Won, J. Rusiecki, J. A. Hoppin, A. Blair, M. R. Bonner, J. H. Lubin, C. Samanic, D. P. Sandler, M. Dosemeci and M. C. R. Alavanja, *Epidemiology*, 2006, **17**, 302–307.
4 M. Strandberg and J. J. Scott-Fordsmand, *Ecotoxicol. Environ. Saf.*, 2004, **57**, 190–201.
5 M. K. Swarcewicz and A. Gregorczyk, *Environ. Monit. Assess.*, 2012, **184**, 3077–3084.
6 X. Zhou, Y. Zhu, Q. Niu, G. Zeng, C. Lai, S. Liu, D. Huang, L. Qin, X. Liu, B. Li, H. Yi, Y. Fu, L. Li, M. Zhang, C. Zhou and J. Liu, *Chem. Eng. J.*, 2021, **416**, 129027.
7 E. D. Visser, N. S. Seroka and L. Khotseng, *Processes*, 2024, **12**, 1111.
8 K. Skic, A. Adamczuk, A. Gryta, P. Boguta, T. Tóth and G. Jozefaciuk, *Sci. Rep.*, 2024, **14**, 30362.

9 P. L. Homagai, M. Bhattarai, K. M. Radhika, K. N. Ghimire, H. Paudyal and A. Bhattarai, *RSC Adv.*, 2022, **12**, 29865–29877.
10 M. A. S. Holanda, J. M. Coelho Menezes, H. D. M. Coutinho and R. N. P. Teixeira, *J. Environ. Manage.*, 2023, **345**, 118719.
11 K. Vidhyarthi, G. Priyadarshi, B. Patel, S. K. Sahu, E. Rami, D. K. Sahoo and A. Patel, *Front. Environ. Sci.*, 2025, **13**, 1674858.
12 G. Priyadarshi, N. P. Raval and M. H. Trivedi, *Int. J. Biol. Macromol.*, 2022, **219**, 53–67.
13 N. P. Raval, G. V. Priyadarshi, S. Mukherjee, H. Zala, D. Fatma, A. Bonilla-Petriciolet, B. L. Abdelmottaleb, L. Duclaux and M. H. Trivedi, *J. Environ. Chem. Eng.*, 2022, **10**(6), 108873.
14 M. Haris, Y. Hamid, M. Usman, L. Wang, A. Saleem, F. Su, J. K. Guo and Y. Li, *J. Hazard. Mater.*, 2021, **416**, 126212.
15 S. N. Ismail, E. m. Ali, B. J. Alwan and A. N. Abd, *Macromol. Symp.*, 2022, **401**(1), 2100312.
16 Z. Anfar, A. Amedlous, A. Ait El Fakir, H. Ait Ahsaine, M. Zbair, S. Lhanafi, R. El Haouti, A. Jada and N. El Alem, *ACS Omega*, 2019, **4**, 9434–9445.
17 A. M. Ayuba and T. A. Nyijime, *J. Mater. Environ. Sci.*, 2021, **2021**, 1.
18 N. T. Ayuba AM, *J. Exp. Res.*, 2021, **9**(2), 1–11.
19 M. T. Amin, A. A. Alazba and M. Shafiq, *Arabian J. Sci. Eng.*, 2018, **43**, 5711–5722.
20 T. A. Nyijime, A. M. Ayuba and H. F. Chahul, *Arabian J. Chem. Environ. Res.*, 2021, **8**(2), 315–335.
21 Z. Anfar, M. Zbair, H. Ait Ahsiane, A. Jada and N. El Alem, *RSC Adv.*, 2020, **10**, 11371–11380.
22 M. Jia, F. Wang, Y. Bian, X. Jin, Y. Song, F. O. Kengara, R. Xu and X. Jiang, *Bioresour. Technol.*, 2013, **136**, 87–93.
23 E. Sterenzon, V. K. Vadivel, Y. Gerchman, T. Luxbacher, R. Narayanan and H. Mamane, *ACS Omega*, 2022, **7**, 118–128.
24 G. V. Priyadarshi, N. P. Raval, D. Barcelo and M. H. Trivedi, *Int. J. Biol. Macromol.*, 2024, **281**, 136279.
25 N. Shah, G. Priyadarshi, B. Patel, S. K. Sahu, M. Joshi, R. Syed, M. Shahid, E. Rami, D. K. Sahoo and A. Patel, *Water Reuse*, 2025, jwrd2025004.
26 H. N. Tran, F. Tomul, N. Thi Hoang Ha, D. T. Nguyen, E. C. Lima, G. T. Le, C. T. Chang, V. Masindi and S. H. Woo, *J. Hazard. Mater.*, 2020, **394**, 122255.
27 Z. Anfar, M. Zbair, H. Ait Ahsiane, A. Jada and N. El Alem, *RSC Adv.*, 2020, **10**, 11371–11380.
28 T. G. Ambaye, M. Vaccari, E. D. van Hullebusch, A. Amrane and S. Rtimi, *Int. J. Environ. Sci. Technol.*, 2021, **18**, 3273–3294.
29 Z. Abbas, S. Ali, M. Rizwan, I. E. Zaheer, A. Malik, M. A. Riaz, M. R. Shahid, M. Z. ur Rehman and M. I. Al-Wabel, *Arabian J. Geosci.*, 2018, **11**(16), 448.
30 Y. Wang, L. Chen, Y. Zhu, W. Fang, Y. Tan, Z. He and H. Liao, *Environ. Sci. Eur.*, 2024, **36**(1), 25.